doi: 10.29382/eqs-2020-0107-01

Inferring seismic hazard in Sichuan-Yunnan region of China based on the modern earthquake catalogue (1980-2019)*

Ziyao Xiong[1] Shiyong Zhou[1,✉] Jiancang Zhuang[2]

[1] *School of Earth and Space Sciences*, *Peking University*, *Beijing*100871, *China*
[2] *The Institute of Statistical Mathematics*, *Tokyo* 1908562, *Japan*

Abstract Based on the modern earthquake catalogue, the incomplete centroidal voronoi tessellation (ICVT) method was used in this study to estimate the seismic hazard in Sichuan-Yunnan region of China. We calculated spatial distributions of the total seismic hazard and background seismic hazard in this area. The Bayesian delaunay tessellation smoothing method put forward by Ogata was used to calculate the spatial distributions of *b*-value. The results show that seismic hazards in Sichuan-Yunnan region are high, and areas with relatively high hazard values are distributed along the main faults, while seismic hazards in Sichuan basin are relatively low.

Keywords: seismic hazard analysis; Voronoi tessellation; spatial smoothing; *b*-value

1 Introduction

The Sichuan-Yunnan region is located in southwest China, which is one of the most active seismic areas in China. Since 1980, there have been several devastating earthquakes with a magnitude of 7.0 or above, including the Lancang M_S7.6 earthquake in 1988, the Sino-Myanmese border-area M_S7.3 earthquake in 1995, the Wenchuan M_S8.0 earthquake in 2008, the Yushu M_S7.1 earthquake in 2010, the Ya'an M_S7.0 earthquake in 2013, and the Jiuzhaigou M_S7.0 earthquake in 2017. The huge casualties and property losses have drawn attentions of seismologists to those areas. In recent years, there have been a large number of seismic studies for this area. For example, based on a study of correlations between crustal deformations and strong earthquakes in Sichuan-Yunnan region, Li et al. (2003) concluded that the key point of seismic hazard predictions in the next few years was the central Sichuan-Yunnan region. A study on strain rate field distribution by Wei et al. (2015) showed that strain rate had a good correlation with earthquakes with a magnitude of above 6.0 in this region. Sun et al. (2014) studied the characteristics of main active faults in this region and showed that the east part of Xiaojiang fault and the middle part of the inner arc belt located in western parts of Yunnan had shown a strong seismicity in recent years. Based on these results, we can have a basic understanding of fault activity characteristics and the distributions of strain rate fields in Sichuan-Yunnan region. However, it is also necessary to understand spatial distributions of seismic hazards in this region as well as its correlations with distributions of faults and strain rate fields. Based on statistical physics, Wang et al. (2013) studied the distribution of seismic hazard in Sichuan-Yunnan region by using the historical seismic catalogue. Different from previous studies, we used the modern seismic catalogue to study seismic hazards. Compared with historical earthquake catalogues or other kinds of data, the modern earthquake catalogue can guarantee more complete and sufficient data to improve the accuracy of calculation results.

In this study, we aimed to estimate long-term seismic hazard in this area based on regional seismicity. Long-term seismic hazard can be obtained based on various types of geophysical observations, such as seismicity, stress/strain fields inferred from earthquake focal mechanisms and crustal deformations (e.g., Vere-Jones, 1978; Ogata,1998; Zhuang et al., 2002; Jiang et al., 2011). In order to comprehensively analyze long-term seismic hazard and distribution characteristics of major earthquakes in this area, the total seismic hazard, background seismic hazard and spatial variations of *b*-value are mainly included in this study.

* **Received** 22 June 2020; **accepted in revised form** 24 July 2020; **published** 17 November 2020.

✉ **Corresponding author. e-mail**: zsy@pku.edu.cn

Total seismic hazard is here defined through the spatial seismicity rate based on all earthquakes in a certain period of time (i.e., including mainshocks and aftershocks). In the study of total seismic hazard, the kernel function estimation method is the most widely used. For example, Vere-Jones (1992), Frankel (1995), Cao et al. (1996) and Jackson and Kagan (1999) used the kernel function estimation method based on a fixed bandwidth. In order to solve the problem of uneven spatial distributions of seismic data, Stock and Smith (2002), Zhuang et al. (2002) and Jiang et al. (2011) proposed different adaptived bandwidth kernel function estimation methods. Compared to kernel functions with a fixed bandwidth, advantages of those with an adaptive bandwidth include that they can avoid over-smoothing high-active seismic areas or under-smoothing aseismic areas.

In addition to the adaptive bandwidth kernel estimation methods, spatial tessellation methods have the same adaptive smoothing function, for example, the Bayesian smoothing method by Ogata et al. (2003) based on Delaunay Tessellation and the Incomplete Centroidal Voronoi Tessellation (ICVT) method by Xiong et al. (2019) based on Voronoi tessellation. Compared with other smoothing methods, ICVT method is easier to implement and has more moderate smooth results. Therefore, in this study, considering the feasibility of calculations and the accuracy of results, we used ICVT method put forward by Xiong et al. (2019) for long-term estimations of the total seismic hazard and studied differences in the spatial distributions of the seismicity.

In order to understand impacts of mainshocks in the region, we further studied background seismic hazard. Because seismicity is clustered and the use of total seismicity may lead to over-estimations of seismic hazard in quiescent period. That is, the total seismic hazard may be predicted too high in aseismic periods, but too low in active periods. We need to distinguish background seismicity from total seismicity by removing aftershocks, that is, declustering. In this study, we adopted the epidemic-type aftershock sequence (ETAS) model based on stochastic declustering (Zhuang et al., 2002; Zhuang, 2011). That is, we calculated probabilities of background seismic events by using ETAS model.

In addition, in order to determine ratios of events between large and small earthquakes, we calculated the *b*-value of Gutenberg and Richter (1944) magnitude-frequency relation (G-R law). Generally, the least square method or the maximum likelihood estimation method was adopted for estimations of *b*-value (Zheng and Zhou, 2014; Zhang and Zhou, 2016). Considering the heterogeneity of spatial distributions of data, we used a Bayesian method with priori smoothness proposed by Ogata et al. (1991) to calculate spatial variations of *b*-value.

2 Tectonic background

Influenced by collisions between the Indian plate and the Eurasian plate, together with northward movements of the Indian Plate, boundaries and interiors of blocks contain tectonic movements such as translations, rotations and uplifts in Sichuan-Yunnan region (Xu et al., 2003). The crustal displacement velocity is strong in the north and west parts, but weak in the south and east parts. Crustal displacements are clockwise rotating around the orogenic junction of the eastern Himalayas and the main body of rhombus block (Qiao et al., 2004).

The faults in this region distribute densely, and active faults are mostly strike-slip faults with inclining slip components (Sun et al., 2014). The faults in this region mainly include Longmenshan fault, Anninghe fault, Zemuhe fault, Xiaojiang fault, Honghe fault, Lancangjiang fault, Nujiang fault, Xianshuihe fault, Litang fault and Yushu fault, etc. (Figure 1).

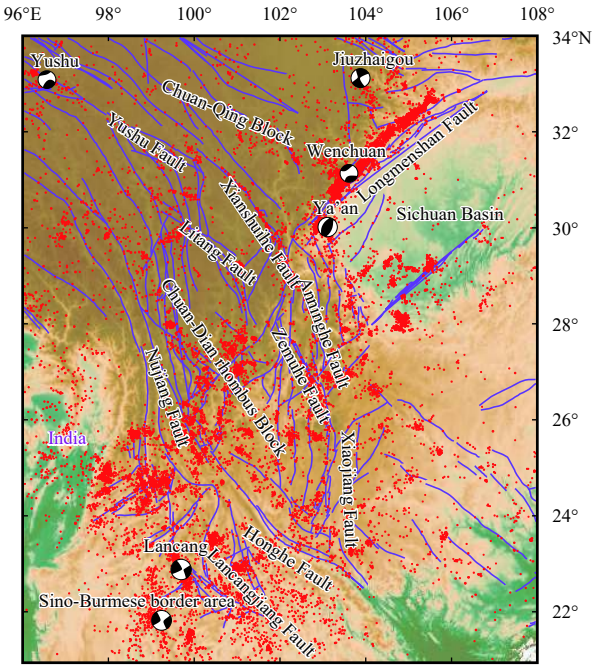

Figure 1 Topographic map of Sichuan-Yunnan region. The purple lines and red dots respectively represent fault traces (reference from Deng et al., 2003) and seismicity with magnitudes higher than 3.0 (from January 1, 1980 to December 1, 2019). And the focal mechanism data is from www.globalcmt.org.

The tectonic loading makes this region prone to earthquakes, where strong earthquake activities are frequent.

Historically, strong earthquakes were mainly distributed on the boundary fault zones of the Chuan-Dian rhombus block and the Chuan-Qing block (Han and Jiang, 2004). In addition, since 1500, there have been 43 earthquakes with a magnitude of M_S7.0 or above occurring in this region, among which the maximum magnitude was M_S8.0.

3 Data

Combined with regional tectonic backgrounds and analyses, we selected 96°E–108°E and 21°N–34°N as scopes of the study areas, and the earthquake catalogue from January 1, 1980 to December 1, 2019. The data of the earthquake catalogue came from the China Earthquake Networks Center (CENC).

When using the modern earthquake catalogue to study the seismic hazard, we usually chose conservative and complete earthquake catalogues to ensure data reliability (Zhou et al., 2018). According to Su et al. (2013) 's analysis on the minimum complete magnitude of earthquake catalogues in Sichuan-Yunnan region, the minimum complete magnitude of this region from 1970 to 1981 was M3.0, which was decreased to M2.5 from 1982 to 2013. In our study, the magnitude-time and the magnitude-frequency relationships of the selected earthquake catalogue are shown in Figure 2. From Figure 2a, there is no obvious earthquake missing in the earthquake catalogue with the magnitude above 3.0. And the significant increase in the number of earthquakes in the earthquake catalogue is the time of the M_S8.0 Wenchuan earthquake in 2008. According to Figure 2b, the accumulative frequencies and non-accumulative frequencies of earthquakes can be fitted as a straight line with changes in magnitude, indicating that magnitude ratios in the earthquake catalogue conform to G-R law. Thus, in this study, earthquake catalogues equal to and above M_S3.0 were adopted, which not only ensured the completeness, but also guaranteed the data quantity.

4 Total seismic hazard

4.1 Method

We used the ICVT method proposed by Xiong et al. (2019) to smooth spatial seismicity due to its easy implementation and the same effectiveness among the best smoothing techniques (Xiong et al. 2019). Voronoi tessellation is a spatial tessellation algorithm proposed by Russian mathematician Georgy Fedoseevich Voronoi in 1908. Through this method, spaces are divided into different Voronoi polygons based on a set of specific points, each of which contains a unique specific point, and any position of a polygon is closer to its specific point than to any other specific point (Tran et al., 2009). In addition, each edge of a Voronoi polygon is a perpendicular bisector between two specific points.

ICVT method is based on centroidal Voronoi tessellation (CVT), that is, given k specific points (x_i,y_i), $i = 1,\ldots,k$, the area of its associated Voronoi polygon is assumed to be S_i, thus we can get the centroid as

$$\begin{pmatrix} x_i^* \\ y_i^* \end{pmatrix} = \int_{S_i} \begin{pmatrix} x \\ y \end{pmatrix} \mathrm{d}x\mathrm{d}y \Big/ \int_{S_i} \mathrm{d}x\mathrm{d}y,\ i = 1,\ldots,k \qquad (1)$$

With the position of the centroid (x_i^*,y_i^*) as the base points, we can obtain a set of new Voronoi polygons.

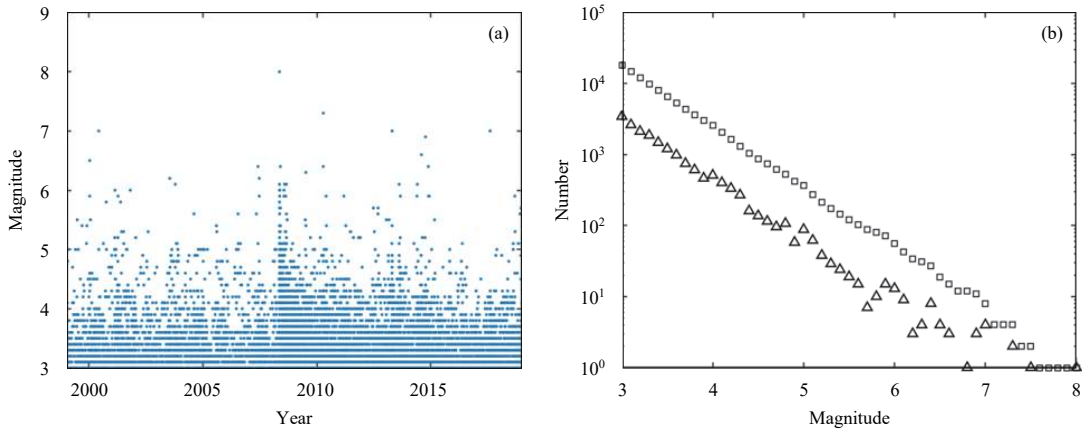

Figure 2 Magnitudes versus times of earthquakes in Sichuan-Yunnan region from January 1, 1980 to December 1, 2019 (a); Magnitude-frequency relationships for Sichuan-Yunnan region earthquakes, from January 1, 1980 to December 1, 2019 (b). The squares and triangles are the cumulative and non-cumulative frequencies of earthquakes that occurred in each magnitude group, respectively

Continually repeat the above operations to update the position of the centroid, and the convergence results can be obtained as

$$\begin{pmatrix} x_i \\ y_i \end{pmatrix} = \begin{pmatrix} x_i^* \\ y_i^* \end{pmatrix}, i = 1, \ldots, k. \quad (2)$$

At this moment, the specific point of each Voronoi polygon is the centroid of that polygon.

According to the above formulas, CVT method is actually a smoothing process based on Voronoi tessellation. Each centroidization process can reduce the difference between adjacent Voronoi cells. However, in the study of seismic hazard, CVT method caused over-smoothing results, so it is necessary to calculate the optimal smoothing times.

In the study of seismic hazard, the first time Voronoi tessellation is calculated based on locations of the earthquake epicenters. Assume that the data set of earthquake epicenters is expressed as $\{(x_i, y_i), i = 1, \ldots, N\}$, where N represents the number of earthquake events, After the tessellation, the seismicity rate of each epicenter is

$$\lambda(x_i, y_i) = \frac{1}{TS_i}, \quad (3)$$

where T represents the study time, and S_i is the area of the i th Voronoi polygon.

After the centroid of each Voronoi polygon was obtained, we calculated the Voronoi tessellation again based on centroid positions, and then repeated the above steps again to obtain the final estimate of earthquake hazard. According to the test by Xiong et al. (2019), it is usually required to be smoothed for twice, that is, the optimal seismicity rate can be obtained through one-step ICVT.

4.2 Results

The original Voronoi tessellation is based on locations of earthquake catalogues, in which the space is divided into many Voronoi polygons, the centroid of each polygon is calculated as shown in Figure 3a. Then, the one-step ICVT is based on the centroids and the final space partitions are as shown in Figure 3b.

By further calculations, spatial hazard distributions are shown in Figure 4. The areas with a high seismicity rate and those area with intensive earthquakes are well matched, which means that the results can accurately reflect the seismic hazards in the corresponding regions. Through smoothing, a good transition was done among the boundaries of different hazard areas. By comparing Figure 4a with Figure 1, it can be seen that regions with a high seismicity rate are basically distributed along the major faults. And the high seismicity areas are concentrated in the vicinity of Yushu fault, Longmenshan fault and Lancangjiang fault, which have occurred strong earthquakes of magnitude 7 or above in the past 30 years, as well as concentrated in the vicinity of Litang fault and Chuan-Dian rhombic block, which have occurred multiple earthquakes of magnitude 6 or above.

5 Background seismic hazard

5.1 Method

Firstly, we used the space-time ETAS model to calculate the probability that an earthquake was a background earthquake. The conditional intensity function of this model is (Ogata and Katsura, 1988; Zhuang et al.,

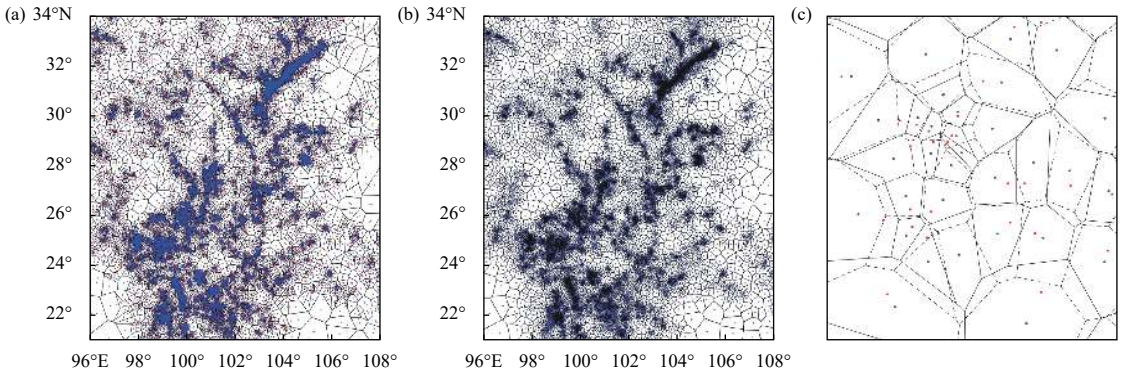

Figure 3 The original Voronoi tessellation of Sichuan-Yunnan region (a). The red dots represent earthquake epicenters and the blue dots are the centroids of the Voronoi cells. The one-step ICVT of Sichuan-Yunnan region (b). The dots represent locations of the base points (i.e., the centroids of the original Voronoi cells). A diagram showing the relationship between the original Voronoi tessellation and the one-step ICVT (c). The solid lines represent the original Voronoi tessellation, and the dotted lines represent the one-step ICVT. The red dots represent earthquake epicenters and the blue dots are the centroids of the original Voronoi cells

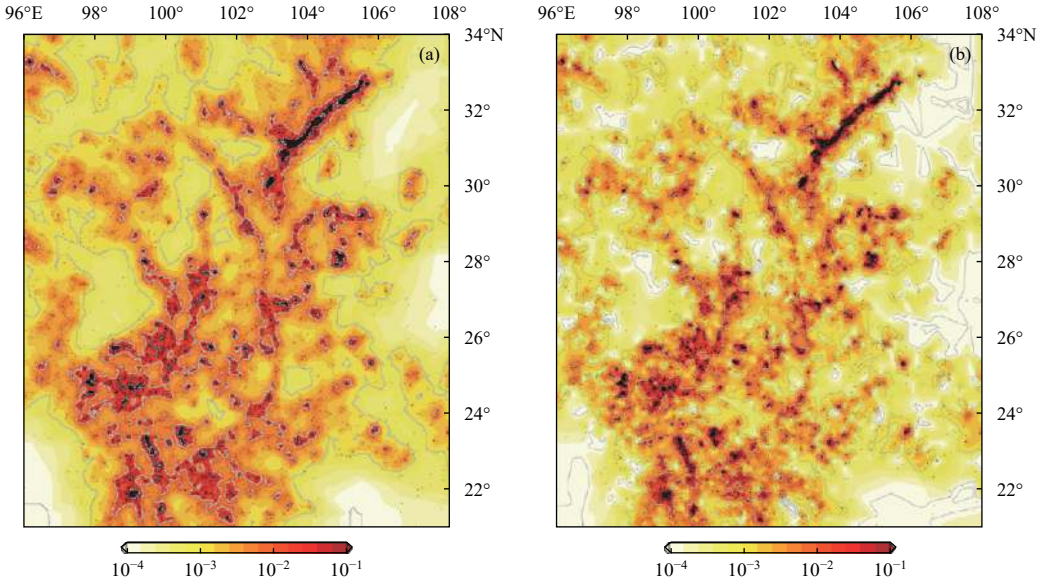

Figure 4 Total seismicity rate (unit: event number·day^{-1}·degree^{-2}) (a). Black points represent earthquake locations. Background seismicity rate (unit: event number·day^{-1}·degree^{-2}) (b). Black points represent earthquake locations

2002; Zhuang, 2011).

$$\lambda(t,x,y|H_t)=\mu(x,y)+\sum_{i:t_i<t}\xi(t,x,y;t_i,x_i,y_i,m_i), \quad (4)$$

in which H_t represents impacts of seismic events in historical seismic activities before the study period and outside the study area; $\mu(x,y)$ represents background seismicity; $\xi(t,x,y;t_i,x_i,y_i,m_i)$ represents contributions of the i th event to subsequent earthquakes, expressed as

$$\xi(t,x,y;t_i,x_i,y_i,m_i)=\kappa(m_i)\,g(t-t_i)\,f(x-x_i,y-y_i;m_i). \quad (5)$$

In the above equations, $\kappa(m)$ is the number of aftershocks triggered by mainshocks with a magnitude of m, m_c represents the magnitude threshold, $g(t)$ is the probability density function of normalized time, and $f(x,y;m)$ is the probability density function of spatial position. The specific forms are expressed as (Zhuang et al., 2005; Ogata and Zhuang, 2006)

$$\kappa(m)=A\exp[\alpha(m-m_c)], \quad m\geq m_c, \quad (6)$$

$$g(t)=\frac{p-1}{c}\left(1+\frac{t}{c}\right)^{-p}, \quad t>0, \quad (7)$$

$$f(x,y;m)=\frac{q-1}{\pi D^2\exp[\gamma(m-m_c)]}\left[1+\frac{x^2+y^2}{D^2\exp[\gamma(m-m_c)]}\right]^{-q}. \quad (8)$$

In calculations, in order to speed up the convergence, $\mu(x,y)=\nu u(x,y)$ is set. Therefore, there are 8 parameters to be estimated, namely $\theta=(\upsilon,A,\alpha,c,p,D,q,\gamma)$. The optimal parameters are obtained by maximizing the logarithmic likelihood function, whose expression is (Daley and Vere-Jones, 2003)

$$\log L(\theta)=\sum_{j:(t_j,x_j,y_j)\in S\times[T_1,T_2]}\log\lambda\left(t_j,x_j,y_j|H_{t_j}\right)-\iint_S\int_{T_1}^{T_1}\lambda(t,x,y|H_t)\,\mathrm{d}t\mathrm{d}x\mathrm{d}y, \quad (9)$$

where S represents the study area, and $[T_1,T_2]$ represents the time range. According to the results of the optimal parameters, the probability that j event is a background earthquake can be obtained as (Zhuang et al., 2002)

$$\varphi_j=\frac{\mu\left(x_j,y_j\right)}{\lambda\left(t_j,x_j,y_j|H_{t_j}\right)}. \quad (10)$$

Background seismicity is calculated in the same way as what is done on total seismicity by smoothing the entire seismic catalogue, but each event is weighted according to the probability that it is a background earthquake. Based on the function φ_j calculated through equation (10), the background seismic hazard can be obtained by using the ICVT model and repeating the steps in Section 3.1.

5.2 Result

According to the above methods, we used earthquake catalogues from January 1, 1980 to December 1, 2019 with magnitudes equal to and above 3.0 again. For data selected in this study, the optimal parameters are $\upsilon=1.010\,2$, $A=0.560\,2$, $\alpha=1.093\,1$, $c=0.003\,2$, $p=1.051\,9$, $D=0.000\,2$, $q=2.167\,0$ and $\gamma=0.883\,4$. The calculated results are shown in Figure 4b, which clearly reflects the distribution of background earthquakes without considering clustering earthquakes. The overall distribution of the

background seismic hazard is similar to that of the total seismic hazard, but the high seismic hazard areas are more concentrated near the fault and seismic zones. This result conforms to the general rule that the total seismic hazard is higher than the background seismic hazard in the whole area.

6 Spatial distribution of *b*-value

The relationship between earthquake frequencies and magnitudes can be expressed as based on the magnitude-frequency relation (Gutenberg and Richter, 1944), $\log_{10}N = a - bM$, where, M represents the earthquake magnitude, N represents the number of earthquakes with magnitude greater than or equal to M, a represents the proportionality constant related to the total seismicity, and b is the b-value of G-R law. In the study of the long-term seismic hazard, b-value plays an important role, which reflects the distribution ratio between large and small earthquakes. The smaller the b-value is, the higher the likelihood of a huge earthquake will be in this area. Moreover, b-value is negatively correlated with the shear stress, so b-value is low in areas with a high stress level (Amitrano, 2003; Schorlemmer et al., 2005).

Here, we used the method of Ogata et al. (2003) to calculate the b-values in this region. (x_i, y_i) was assumed as the location of an earthquake, and we adopted a linear difference algorithm to obtain values of other locations in this space, so the function at any location can be obtained through

$$a_1 x_i + a_2 x_j + a_3 x_k = x,$$

$$a_1 y_i + a_2 y_j + a_3 y_k = y,$$

$$a_1 + a_2 + a_3 = 1, \tag{11}$$

$$\phi(x,y) = a_1\phi_i + a_2\phi_j + a_3\phi_k, \tag{12}$$

in which (i, j, k) represent indices of seismic events with epicenters at the vertices of Delaunay triangle, a_1, a_2, and a_3 represent coefficients of each difference algorithm. Then we can estimate b-values of all points based on the above spatial relations.

Suppose that the magnitude of an earthquake event at (x_i, y_i) is M_i, $i = 1, 2, \ldots, N$, then the likelihood function of the parameter θ can be expressed as

$$L(\beta_\theta) = \prod_{i=1}^{N} b_\theta(x_i, y_i)\, 10^{-b_\theta(x_i,y_i)(M_i - M_c)}, \tag{13}$$

where, $M_i > M_c$, and the specific form of b-value is

$$b_\theta(x,y) = e^{\phi_\theta(x,y)}. \tag{14}$$

Since the dimension of the parameter is the same as the data point, θ must be restricted. Here, the penalty log-likelihood function is (Good and Gaskins, 1971)

$$R(\theta|w) = \ln L(\theta) - Q(\theta|w), \tag{15}$$

where the roughness of θ is

$$Q(\theta|w) = w \iint_A \left[\left(\frac{\partial \beta_\theta(x,y)}{\partial x} \right)^2 + \left(\frac{\partial \beta_\theta(x,y)}{\partial y} \right)^2 \right] \mathrm{d}x\mathrm{d}y, \tag{16}$$

and w is a hyper-parameter to be estimated. Based on Bayesian method, the prior probability density of θ is

$$\pi(\theta|w) = \frac{\mathrm{e}^{-Q(\theta|w)}}{\int_\Theta \mathrm{e}^{-Q(\theta|w)}\mathrm{d}\theta} \tag{17}$$

Therefore, the function of joint probability density of observed data and parameter θ is

$$p(\theta; data) = L(\theta)\pi(\theta|w), \tag{18}$$

The function of posterior probability density is

$$p(\theta|w) = \frac{L(\theta)\pi(\theta|w)}{\Lambda(w)} \tag{19}$$

And the function of unconditional probability density of observed data is

$$\Lambda(w) = \int_\Theta L(\theta)\pi(\theta|w)\,\mathrm{d}\theta. \tag{20}$$

Finally, the Akaike Bayesian Information Criterion (ABIC) proposed by Akaike (1980) was used to get the optimal parameters. The optimal spatial distribution of b-value can be obtained through parameters corresponding to the minimum ABIC.

The calculation of this part uses the earthquake catalogue from January 1, 1980 to December 1, 2019 with magnitude equal to and above 3.0, and the results are shown in Figure 5. The calculated results are basically consistent with distributions of large and small earthquakes, and areas with a low b-value are distributed along the faults. Due to the b-value reflects the distribution ratio between large and small earthquakes, a number of studies have shown that the low b-value region has a high seismic hazard. For example, Pailoplee et al. (2013) studied the potential areas of upcoming earthquakes along the Northern segment of the Sumatra-Andaman subduction zone. The results shown that the regions with low b-values were in good agreement with the locations of the subsequent earthquakes. Li and Zhou (2014) found that the initial rupture point of the Wenchuan earthquake was located in the low-b-value region, the rupture termination place was located in the high-b-value region, and the maximum displacement segment generated in Beichuan after the Wenchuan earthquake was also in a low b-value region. In this research, b-values in the central and northwestern Sichuan-Yunnan region and the vicinity of Longmenshan fault zone are relatively low, indicating a

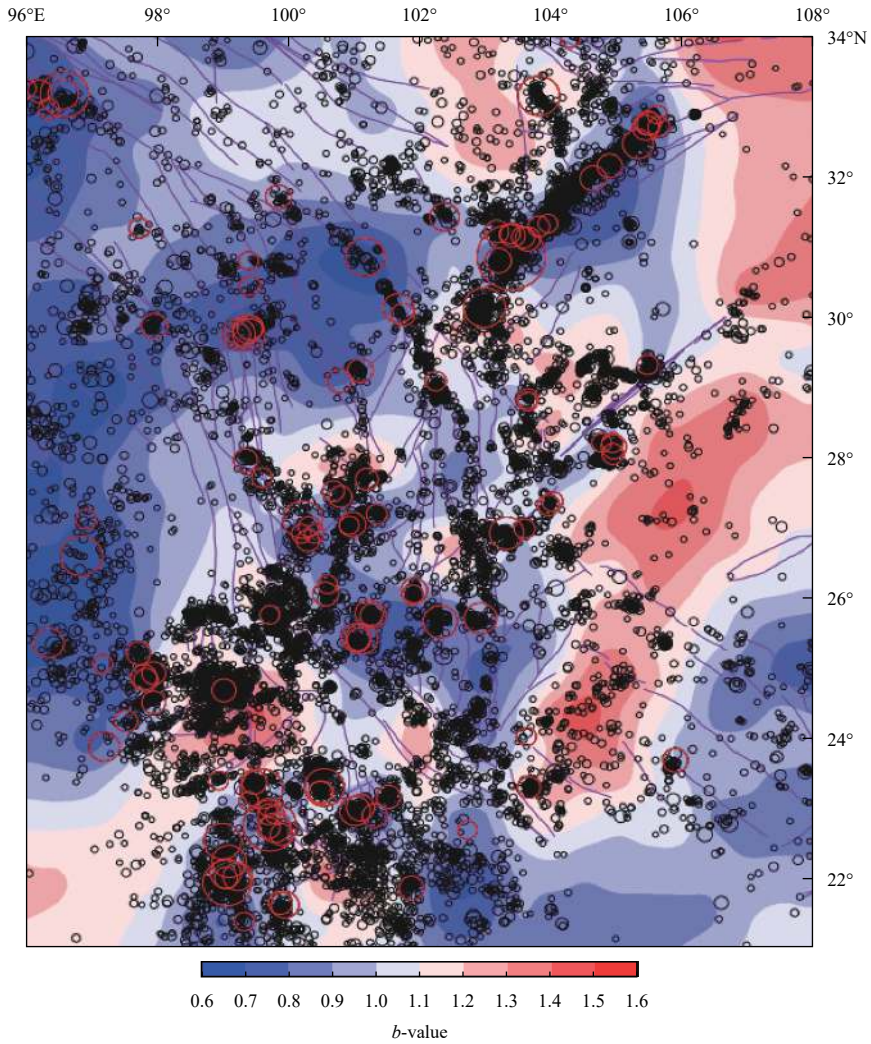

Figure 5 Spatial variations of *b*-value in Sichuan-Yunnan region. Black points represent locations of earthquake epicenters, and red circles mark the epicenters of earthquakes with a magnitude of 5.5 or above. The sizes of the circles represent earthquake magnitudes, from the smallest 3.0 to the largest 7.8. The purple lines represent traces of faults

high possibility of strong earthquakes. The *b*-values in eastern Sichuan-Yunnan region are relatively high, indicating a low risk of strong earthquakes. In addition, the overall *b*-values of Sichuan basin are high, except for the southwest of Sichuan basin.

7 Discussion and conclusions

7.1 Discussion

Comparing with previous studies on the seismic hazard in Sichuan-Yunnan region by using different methods, we found some researches on seismic hazard are based on engineering seismology. For example, Liu et al. (2020) studied the seismic hazard of Xiaojiang fault zone by using scenario earthquakes, combining with characteristics of previous ruptures and geometric structures of the fault, and calculated the peak ground acceleration (PGA) along the fault. The results show that PGA along the fault line is higher than that in other areas. This kind of research is more about short-term estimations of the seismic hazard in a small area. Whereas, our results are more conducive to long-term estimations of seismic activities in large regions. That is, our results can directly reflect spatial seismicity rates in recent decades and are conducive to predictions of large earthquakes.

There are also some studies based on statistical methods in this area. For example, Wang et al. (2013) studied distributions of seismic hazard in Sichuan-Yunnan region based on a historical seismic catalogue. This study used an earthquake catalogues with different time and magnitude ranges from ours. Comparing with the results, our results of seismic hazard have more moderate spatial

smoothing results and can better reflect the recent seismic activities. In addition, the spatial variations of *b*-values calculated by our study can help us better understand the high-risk areas of strong earthquakes.

7.2 Conclusions

Based on data of seismic catalogues, this study mainly estimates the seismic hazard of Sichuan-Yunnan region from the perspective of statistical analysis. The data from 1980 to 2019 of modern earthquake catalogue was used in this study, which has advantages including complete earthquake catalogue records, a higher accuracy than historical earthquake catalogues, as well as a larger number of earthquakes in the recent 30 years. Therefore, long-term seismic hazard in this region can be accurately estimated.

According to analyses of the results obtained through ICVT method, the whole Sichuan-Yunnan region has a high seismic hazard, in which high-value areas are concentrated near major faults, while Sichuan basin area has a relatively low seismic hazard.

According to research results of background seismic hazard, the areas with high background seismicity values are smaller than those with high total seismicity values, which are more concentrated near the strong earthquakes and active fault zones.

Analyses of the spatial variations of *b*-values show that the range of *b*-values in this region is mainly between 0.6 and 1.6. In conclusion, the overall *b*-values in the Sichuan-Yunnan region are low, indicating a high likelihood of strong earthquakes. The *b*-values are relatively high in Sichuan basin and east parts of Sichuan-Yunnan region, showing a low likelihood of strong earthquakes.

In summary, our simulation results summarize seismic activity patterns in the Sichuan-Yunnan region from 1980 to 2019. The seismic hazard results and *b*-value results can provide references for high-hazard seismic regions and those with high-probability occurrences of strong earthquakes. Furthermore, the calculation results of seismic hazard and *b*-value can be used to simulate seismic catalogues and estimate seismicity rates of strong earthquakes. The above information can also provide references for future researches on seismic hazard in this area.

Acknowledgments

This research was jointly supported by Ningxia Hui Autonomous Region Key R&D Plan East West cooperation Project (No. 2018BFG02011), National Natural Science Foundation of China (No. 41674047) and China Earthquake Science Experiment Site Project, CEA (Nos. 2019CSES0105 and 2019CSES0106).

References

Akaike H (1980) Likelihood and Bayes procedure, in Bayesian Statistics. In: Bernard JM, DeGroot MH, Lindley DV and Smith AFM eds. Valencia, Spain, Valencia University Press, pp.1–13

Amitrano D (2003) Brittle-ductile transition and associated seismicity: Experimental and numerical studies and relationship with the *b*-value. J Geophys Res **108**(B1): 2044

Cao TQ, Petersen MD and Reichle MS (1996) Seismic hazard estimate from background seismicity in Southern California. Bull Seismol Soc Amer **86**(5): 1372–1381

Daley DD and Vere-Jones D (2003) An Introduction to Theory of Point Processes—Volume 1: Elementrary Theory and Methods, Second Edition. New York, Springer, pp.211–275

Deng QD, Zhang PZ, Ran YK, Yang XP, Min W and Chen LC (2003) Active tectonics and earthquake activities in China. Earth Science Frontiers **10**(S1): 66–73

Frankel A (1995) Mapping seismic hazard in the central and eastern United States. Seismol Res Lett **66**: 8–21

Good IJ and Gaskins RA (1971) Nonparametric roughness penalties for probability densities. Biometrika **58**: 255–277

Gutenberg R and Richter CF (1944) Frequency of earthquakes in California. Bull Seismol Soc Amer **34**: 185–188

Han WB and Jiang GF (2004) Study on distribution characteristics of strong earthquakes in Sichuan-Yunnan area and their geological tectonic background. Acta Seismologica Sinica **26**(2): 221–222 (in Chinese with English abstract)

Jackson DD and KaganYY (1999) Testable earthquake forecasts for 1999. Seismol Res Lett **70**(4): 393–403

Jiang MM, Zhou SY, Chen YJ and Ai Y (2011) A new multidimensional stress release statistical model based on coseismic stress transfer. Geophys J Int **187**: 1479–1494

Li TM, Deng ZH and Lv YP (2003) Research on the crustal deformation data related to characteristics of strong earthquake (M_S≥6.0) distribution in the area of Chuandian (Sichuan-Yunnan), China. Earthquake Research in China **19**(2): 132–147 (in Chinese with English abstract)

Li ZF and Zhou BG (2014) Asperity identification based on low *b*-value: Application to the Longmenshan and Xianshuihe Fault Zone. Technology for Earthquake Disaster Prevention **9**(2): 213–225 (in Chinese with English abstract)

Liu JW, Zhang LF and Du Y (2020) Seismic hazard assessment of the mid-northern segment of Xiaojiang fault zone in southwestern China using scenario earthquakes. Bull Seismol Soc Amer **110**(3)

Ogata Y (1998) Space-time point-process models for earthquake occurrences. Annals of the Institute of Statistical Mathematics **50**(2): 379–402

Ogata Y, Imoto M and Katsura K (1991) 3D spatial variation of *b*-values of magnitude frequency distribution beneath the Kanto District, Japan. Geophys J Int **104**(1): 135–146

Ogata Y and Katsura K (1988) Likelihood analysis of spatial

inhomogeneity for marked point patterns. Ann Inst Stat Math **40**: 29–39

Ogata Y, Katsura K and Tanemura M (2003) Modelling heterogeneous space-time occurrences of earthquakes and its residual analysis. Appl Stat (JRSSC) **52**: 499–509

Ogata Y and Zhuang JC (2006) Space-time ETAS models and an improved extension. Tectonophysics **413**: 13–23

Pailoplee S, Surakiatchai P and Charusiri P (2013) *b*-value anomalies along the northern segment of the Sumatra-Andaman subduction zone: Implications for upcoming earthquakes. Journal of Earthquake and Tsunami **7**(04): 1350030

Qiao XJ, Wang Q and Du RL (2004) Characteristics of current crustal deformation of active blocks in the Sichuan-Yunnan region. Chin J Geophys **47**(5): 805–811 (in Chinese with English abstract)

Schorlemmer D, Wiemer S and Wyss M (2005) Variations in earthquake size distribution across different stress regimes. Nature **437**(7058): 539–542

Stock C and Smith EGC (2002) Adaptive kernel estimation and continuous probability representation of historical earthquake catalogs. Bull Seismol Soc Amer **92**(3): 904–912

Su YJ, Li YL, Li ZH, Yi GX, and Liu LF (2013) Analysis of minimum complete magnitude of earthquake catalog in Sichuan-Yunnan region. Journal of Seismological Research **26** (Suppl.): 10–16 (in Chinese with English abstract)

Sun Y, Wu ZH, An MJ and Long CX (2014) Activity characteristics of primary active faults in Yunnan-Sichuan area and their seismic activity in the past. China Earthquake Engineering Journal **36**(2): 320–330 (in Chinese with English abstract)

Tran QT, Tainar D and Safar M (2009) Transactions on Large-Scale Data and Knowledge-Centered Systems. Berlin-Heidelberg, Springer, p.357

Vere-Jones D (1978) Earthquake prediction–A statistician's view. Earth Planets and Space **26**(2): 129–146

Vere-Jones D (1992) Statistical methods for the description and display of earthquake catalogs. In Walden AT and Guttorp P eds. Statistics in the Environmental and Earth Sciences. London, Arnold Publishers, pp.220–246

Wang F, Shen ZK, Wang M, Wang YZ and Tao W (2013) Seismic hazard analysis of the Sichuan-Yunnan region, western China. Seismol Geol **35**(1): 102–111 (in Chinese with English abstract)

Wei WX, Jiang ZS, Liu XX and Zou ZY (2015) Distribution and variation characteristics of strain rate field in the Sichuan-Yunnan region. Earthquake **35**(4): 11–20 (in Chinese with English abstract)

Xiong ZY, Zhuang JC and Zhou SY (2019) Long-term earthquake hazard in North China estimated from a modern catalog. Bull Seismol Soc Amer **109**(6): 2340–2355

Xu XW, Wen XZ, Zheng RZ, Ma WT, Song FM and Yu GH (2003) The latest tectonic variation pattern of the active block in Sichuan-Yunnan area and its dynamic source. Science in China (Series D) **33**: 151–162

Zhang SJ and Zhou SY (2016) Spatial and temporal variation of *b*-values in Southwest China. Pure Appl Geophys **173**: 85–96

Zheng YJ and Zhou SY (2014) The spatiotemporal variation of the *b*-value and its tectonic implications in North China. Earthq Sci **27**(3): 301–310

Zhou YJ, Zhou SY and Zhuang JC (2018) A test on methods for MC estimation based on earthquake catalog. Earth Planet Phys **2**: 150–162

Zhuang JC (2011) Next-day earthquake forecasts for the Japan region generated by the ETAS model by using the ETAS model. Earth Planets and Space **63**: 207–216

Zhuang JC, Chang C-P, Ogata Y and Chen Y-I (2005) A study on the background and clustering seismicity in the Taiwan region by using point process models. J Geophys Res **110**(B5): 1978–2012

Zhuang JC, Ogata Y and Vere-Jones D (2002) Stochastic delustering of space-time earthquake occurrences. J Am Stat Assoc **97**: 369–380